REFERENCES

[1] S. Peleg and B. Friedlander, "The discrete polynomial-phase transform," *IEEE Trans. Signal Process.*, vol. 43, no. 8, pp. 1901–1914, Aug. 1995.

[2] S. Barbarossa, A. Scaglione, and G. B. Giannakis, "Product high-order ambiguity function for multicomponent polynomial-phase signal modeling," *IEEE Trans. Signal Process.*, vol. 46, no. 3, pp. 691–708, Mar. 1998.

[3] B. Boashash and P. O'Shea, "Polynomial Wigner-Ville distributions and their relationship to time-varying higher order spectra," *IEEE Trans. Signal Process.*, vol. 42, no. 1, pp. 216–220, Jan. 1994.

[4] M. Benidir and A. Ouldali, "Polynomial phase signal analysis based on the polynomial derivatives decompositions," *IEEE Trans. Signal Process.*, vol. 47, no. 7, pp. 1954–1965, Jul. 1999.

[5] B. Barkat and B. Boashash, "Design of higher order polynomial Wigner-Ville distributions," *IEEE Trans. Signal Process.*, vol. 47, no. 9, pp. 2608–2611, Sep. 1999.

[6] P. O'Shea, "A new technique for instantaneous frequency rate estimation," *IEEE Signal Process. Lett.*, vol. 9, no. 8, pp. 251–252, Aug. 2002.

[7] ——, "A fast algorithm for estimating the parameters of a quadratic FM signal," *IEEE Trans. Signal Process.*, vol. 52, no. 2, pp. 385–393, Feb. 2004.

[8] J. Angeby, "Estimating signal parameters using the nonlinear instantaneous least squares approach," *IEEE Trans. Signal Process.*, vol. 48, no. 10, pp. 2721–2732, Oct. 2000.

[9] T. Abatzoglou, "Fast maximum likelihood joint estimation of frequency and frequency rate," in *Proc. IEEE Int. Conf. ICASSP*, 1986.

[10] S. Peleg and B. Porat, "Linear FM signal parameter estimation from discrete-time observations," *IEEE Trans. Aerosp. Electron. Syst.*, vol. 27, no. 4, pp. 607–616, Jul. 1991.

Estimating Statistical Properties of Eddy-Current Signals From Steam Generator Tubes

Aleksandar Dògandžić and Ping Xiang

***Abstract*—We develop a model for characterizing amplitude and phase probability distributions of eddy-current signals and propose a maximum likelihood (ML) method for estimating the amplitude and phase distribution parameters from measurements corrupted by additive complex white Gaussian noise. The squared amplitudes and phases of the potential defect signals are modeled as independent, identically distributed (i.i.d.) random variables following gamma and von Mises distributions, respectively. Newton–Raphson iteration is utilized to compute the ML estimates of the unknown parameters. We also compute Cramér–Rao bounds (CRBs) for the unknown parameters and discuss initialization of the Newton–Raphson iteration. The proposed method is applied to analyze rotating-probe eddy-current data from steam-generator tube inspection in nuclear power plants. The obtained estimates can be utilized for maximum *a posteriori* (MAP) signal phase and amplitude estimation, as well as efficient feature extractors in a defect classification scheme. We present numerical examples with both real and simulated data to demonstrate the performance of the proposed methods.**

***Index Terms*—Eddy-current signal modeling, maximum likelihood parameter estimation, Newton–Raphson iteration.**

I. INTRODUCTION

In eddy-current based nondestructive evaluation of materials, a flaw is usually detected by observing probe impedance changes caused by the interaction between induced oscillating electric current in a conductor and a defect [1], [2]. Eddy-current inspection is performed extensively to detect and size flaws in steam-generator tubes in nuclear power plants [3], [4]. Rotating-probe eddy-current testing has been proposed to improve the detection, interpretation, and sizing of defects [3]. (For related analytical and numerical solutions to the eddy-current testing problem, see, e.g., [1], [5]–[8], and references therein.) Rotating probes usually consist of three coils spaced $2\pi/3$ rad (120°) apart, as shown in Fig. 1. Each coil scans the inner surface of the tube by moving along a helical path. To extract meaningful information from the rotating-probe data, a preprocessing step is performed first [4]. The raw data is one-dimensional (1-D) in nature, and a synchronization step converts it to a two-dimensional (2-D) image, where each column of the resulting image contains the data from one rotation. Fig. 2 illustrates the result of this process. Fig. 2(a) and (b) show the raw 1-D signal and synchronized 2-D image, respectively. Fig. 2(c) is a result of calibration where potential defect signals show up; the details of the calibration process are described in [4]. In Fig. 3, we present impedance-plane plots of typical signals measured by the rotating-probe eddy-current system. Further analysis of the potential defect signals is needed to discriminate between defects and nondefects, as well as between different kinds of defects. In this correspondence (see also [9]), we propose a statistical model for characterizing amplitude and phase probability distributions of eddy-current signals. We model the squared amplitudes and

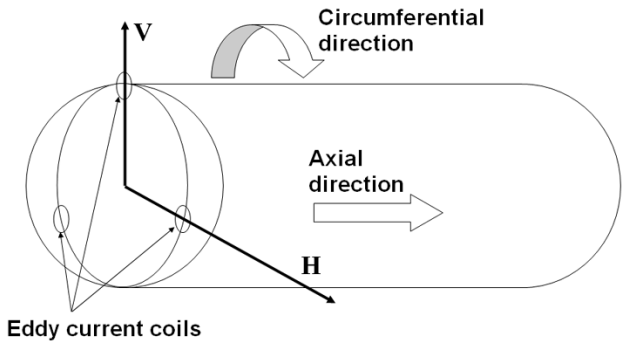

Fig. 1. Rotating-probe eddy-current system.

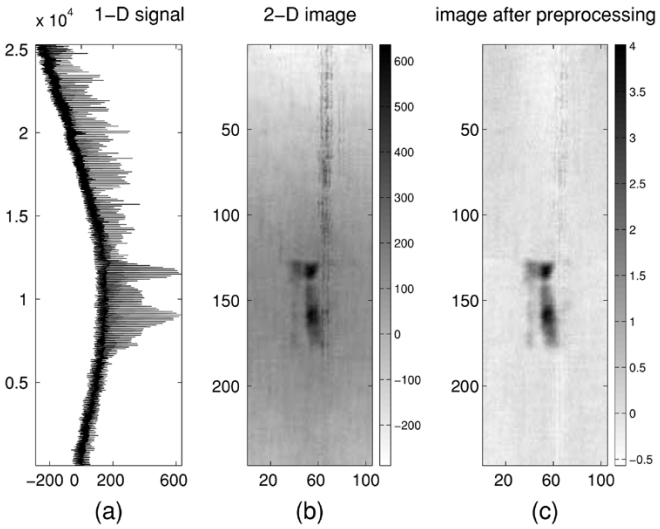

Fig. 2. Signal preprocessing. (a) 1-D raw data. (b) 2-D image. (c) 2-D image after preprocessing.

Manuscript received June 8, 2004; revised November 2, 2004. This work was supported by the NSF Industry-University Cooperative Research Program, Center for Nondestructive Evaluation, Iowa State University. The associate editor coordinating the review of this manuscript and approving it for publication was Prof. Tulay Adali.

The authors are with the ECpE, Department of Electrical and Computer Engineering, Iowa State University, Ames, IA 50011 USA (e-mail: ald@iastate.edu; pxiang@iastate.edu).

Digital Object Identifier 10.1109/TSP.2005.851173

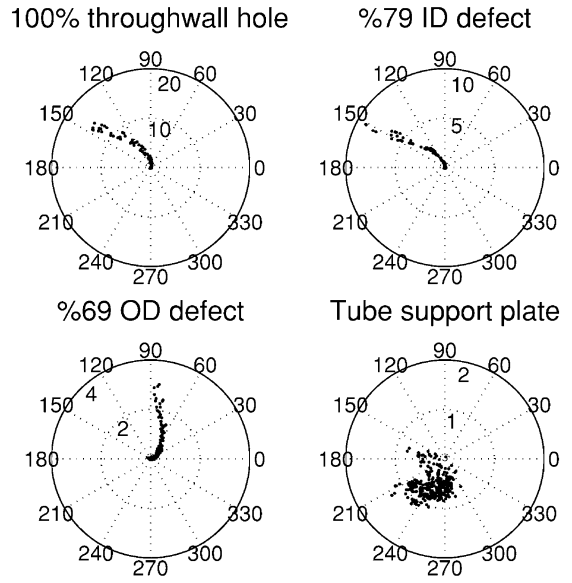

Fig. 3. Signals from different discontinuities in impedance plane.

phases of the potential defect signals as independent, identically distributed (i.i.d.) random variables following gamma and von Mises distributions, respectively, and derive a maximum likelihood (ML) method for estimating the unknown amplitude and phase distribution parameters from noisy measurements. We also develop a maximum *a posteriori* (MAP) estimator of the signal amplitudes and phases.

The proposed statistical model and ML estimation algorithm are generally applicable to measurement scenarios where signal amplitudes and phases have *unimodal distributions*. For example, the proposed ML method can be used to estimate the statistical properties of communication channels. Once estimated, these properties can be incorporated into the receiver design, along the lines of, e.g., [10].

In Section II, we introduce the signal and noise models. The Newton–Raphson algorithm for the ML estimation is presented in Section III, its initialization is discussed in Section III-A, and Cramér–Rao bounds (CRBs) for the unknown parameters are presented in Section III-B. The MAP method for estimating the signal amplitudes and phases is described in Section IV. We apply the proposed ML method to analyze rotating-probe eddy-current data from steam-generator tube inspections and evaluate its accuracy via numerical simulations; see Section V. In Section V, we also utilize an empirical-Bayes MAP method to estimate the signal amplitudes and phases from noisy measurements. Concluding remarks are given in Section VI.

II. Signal and Noise Models

Characterizing the amplitude and phase probability distributions of eddy-current signals is important for flaw detection and classification. For example, after preprocessing and calibration of rotating-probe eddy-current data, the true defect signals should have sufficiently large amplitudes (compared with the noise level), and their phases should lie in the first and second quadrants of the impedance plane (i.e., between 0 and π rad); see [4]. The phase information is also essential for discriminating between inner diameter (ID) and outer diameter (OD) defects; see [4] and Fig. 3. (Note that the defect signals in Fig. 3 were collected from machined defects in a low-noise environment.) Below, we describe a statistical model for characterizing the amplitude and phase probability distributions of the potential defects.

Assume that we have collected K complex eddy-current measurements $y_k,\ k = 1, 2, \ldots, K$ from neighboring spatial locations. These measurements are modeled as

$$y_k = \sqrt{\alpha_k} \cdot e^{j\beta_k} + e_k, \quad k = 1, 2, \ldots, K \tag{1}$$

where

i) $\alpha_k,\ k = 1, 2, \ldots, K$ are i.i.d. squared signal amplitudes (powers) following a *gamma distribution* with the probability density function (pdf)

$$p_\alpha(\alpha_k; a, b) = \frac{b^a}{\Gamma(a)} \cdot \alpha_k^{a-1} \exp(-b\alpha_k), \quad \alpha_k \geq 0 \tag{2}$$

where $a, b > 0$. (Interestingly, in the special case where $a = 1$, the amplitudes $\sqrt{\alpha_k}$ follow a Rayleigh distribution.)

ii) $\beta_k,\ k = 1, 2, \ldots, K$ are i.i.d. signal phases, independent of the amplitudes, which follow a *von Mises distribution* described by the pdf (see [11]):

$$p_\beta(\beta_k; c, d) = \frac{1}{2\pi I_0(d)} \cdot \exp[d\cos(\beta_k - c)], \quad 0 < \beta_k \leq 2\pi \tag{3}$$

where c and $d > 0$ can be viewed as the mean and variance parameters, respectively, and $I_0(\cdot)$ denotes the modified Bessel function of the first kind and order zero[1] (In the special case where $d = 1$, it simplifies to the uniform distribution on the interval $[0, 2\pi]$.)

iii) $e_k,\ k = 1, 2, \ldots, K$ are i.i.d. zero-mean *complex Gaussian noise samples* independent of the signal amplitudes and phases having known variance σ^2. (The noise variance σ^2 can be estimated from the neighboring measurement locations that contain only noise.)

Our goal is to find the ML estimates of the unknown model parameters a, b, c, and d using the observations $y_k,\ k = 1, 2, \ldots, K$.

Define the vector of unknown parameters

$$\boldsymbol{\lambda} = [a, b, c, d]^T$$

and the vectors of signal amplitudes and phases

$$\boldsymbol{\theta}_k = [\alpha_k, \beta_k]^T, \quad k = 1, 2, \ldots, K$$

where "T" denotes a transpose. The assumptions iii) and (1) imply that the conditional pdf of y_k given $\boldsymbol{\theta}_k$ is complex Gaussian:

$$p_{y|\boldsymbol{\theta}}(y_k|\boldsymbol{\theta}_k) = \frac{1}{\pi\sigma^2} \exp\left(-\frac{|y_k - \sqrt{\alpha_k}e^{j\beta_k}|^2}{\sigma^2}\right) \tag{4}$$

and, due to the assumed independence of the signal amplitudes and phases, the pdf of the $\boldsymbol{\theta}_k$ is

$$p_{\boldsymbol{\theta}}(\boldsymbol{\theta}_k; \boldsymbol{\lambda}) = p_\alpha(\alpha_k; a, b) \cdot p_\beta(\beta_k; c, d). \tag{5}$$

The marginal distribution of y_k is then obtained by integrating out the signal power α_k and phase β_k:

$$\begin{aligned} p_y(y_k; \boldsymbol{\lambda}) &= \int_\Theta p_{y|\boldsymbol{\theta}}(y_k|\boldsymbol{\theta}) p_{\boldsymbol{\theta}}(\boldsymbol{\theta}; \boldsymbol{\lambda}) d\boldsymbol{\theta} \\ &= \frac{1}{\pi\sigma^2} \int_0^{2\pi} d\beta \int_0^\infty \exp\left(-\frac{|y_k - \sqrt{\alpha}e^{j\beta}|^2}{\sigma^2}\right) \\ &\quad \cdot p_\alpha(\alpha; a, b) p_\beta(\beta; c, d) d\alpha \end{aligned} \tag{6}$$

[1]The von Mises distribution is one of the most used distributions for modeling random phase and is analogous to the normal distributions on the real line. It is also known as the Tikhonov distribution in the communications literature, see, e.g., [10], [12, (3.37)] , and ([13, (6.1)].

where $\boldsymbol{\Theta} = \{(\alpha, \beta) : 0 < \alpha, 0 < \beta \leq 2\pi\}$. Maximizing the log-likelihood function of $\boldsymbol{\lambda}$ for all available measurements

$$\boldsymbol{y} = [y_1, y_2, \ldots, y_K]^T$$

yields the ML estimate of $\boldsymbol{\lambda}$:

$$L(\boldsymbol{\lambda}, \boldsymbol{y}) = \sum_{k=1}^{K} \ln p_y(y_k; \boldsymbol{\lambda}). \tag{7}$$

The difficulty in estimating $\boldsymbol{\lambda}$ arises due to the integral form of the density function (6). In the following, we present the Newton–Raphson method for computing the ML estimates of $\boldsymbol{\lambda}$.

III. Maximum Likelihood Estimation

We derive the Newton–Raphson algorithm for maximizing (7). The gradient vector $\partial L(\boldsymbol{\lambda}, \mathbf{y})/\partial \boldsymbol{\lambda}$ and Hessian matrix $\partial^2 L(\boldsymbol{\lambda}, \mathbf{y})/\partial \boldsymbol{\lambda} \partial \boldsymbol{\lambda}^T$ are

$$\frac{\partial L(\boldsymbol{\lambda}, \boldsymbol{y})}{\partial \boldsymbol{\lambda}} = \sum_{k=1}^{K} \frac{\partial \ln p_y(y_k; \boldsymbol{\lambda})}{\partial \boldsymbol{\lambda}} \tag{8a}$$

$$\frac{\partial^2 L(\boldsymbol{\lambda}, \mathbf{y})}{\partial \boldsymbol{\lambda} \partial \boldsymbol{\lambda}^T} = \sum_{k=1}^{K} \frac{\partial^2 \ln p_y(y_k; \boldsymbol{\lambda})}{\partial \boldsymbol{\lambda} \partial \boldsymbol{\lambda}^T} \tag{8b}$$

where the terms in the above summations have been computed using the following formulas:

$$\begin{aligned} &\frac{\partial}{\partial \lambda_i}\{\ln p_y(y_k; \boldsymbol{\lambda})\} \\ &\quad = [p_y(y_k; \boldsymbol{\lambda})]^{-1} \cdot \int_{\boldsymbol{\Theta}} p_{y|\boldsymbol{\theta}}(y_k|\boldsymbol{\theta}) \frac{\partial p_\theta(\boldsymbol{\theta}; \boldsymbol{\lambda})}{\partial \lambda_i} d\boldsymbol{\theta} \end{aligned} \tag{9a}$$

$$\begin{aligned} &\frac{\partial^2}{\partial \lambda_i \partial \lambda_m}\{\ln p_y(y_k; \boldsymbol{\lambda})\} \\ &\quad = [p_y(y_k; \boldsymbol{\lambda})]^{-1} \cdot \int_{\boldsymbol{\Theta}} p_{y|\boldsymbol{\theta}}(y_k|\boldsymbol{\theta}) \frac{\partial^2 p_\theta(\boldsymbol{\theta}; \boldsymbol{\lambda})}{\partial \lambda_i \partial \lambda_m} d\boldsymbol{\theta} \\ &\qquad - [p_y(y_k; \boldsymbol{\lambda})]^{-2} \cdot \int_{\boldsymbol{\Theta}} p_{y|\boldsymbol{\theta}}(y_k|\boldsymbol{\theta}) \frac{\partial p_\theta(\boldsymbol{\theta}; \boldsymbol{\lambda})}{\partial \lambda_i} d\boldsymbol{\theta} \\ &\qquad \cdot \int_{\boldsymbol{\Theta}} p_{y|\boldsymbol{\theta}}(y_k|\boldsymbol{\theta}) \frac{\partial p_\theta(\boldsymbol{\theta}; \boldsymbol{\lambda})}{\partial \lambda_m} d\boldsymbol{\theta} \end{aligned} \tag{9b}$$

for $i, m = 1, 2, 3, 4$ and $k = 1, 2, \ldots, K$. After applying the change-of-variable transformation

$$u = b\alpha \tag{10}$$

the above integral expressions can be easily computed using Gauss quadratures. (The Gauss quadrature formulas and their application to statistics are discussed in detail in [14, ch. 5.3].) We applied the Gauss–Chebyshev and generalized Gauss–Laguerre quadratures (of orders N_{C} and N_{L}) to approximate integrals over β and u, respectively, yielding

$$\begin{aligned} &\int_0^{2\pi} d\beta \int_0^{\infty} f(u, \beta) u^{a-1} \exp(-u) du \\ &\qquad \approx \frac{2\pi}{N_{\mathrm{C}}} \sum_{n=1}^{N_{\mathrm{C}}} \sum_{i=1}^{N_{\mathrm{L}}} w_i(a-1) f(u_i(a-1), \beta_n) \end{aligned} \tag{11}$$

where $f(u, \beta)$ is an arbitrary real function, $u_i(a-1)$ and $w_i(a-1)$ are the abscissas and weights of the generalized Gauss–Laguerre quadrature of order N_{L} with parameter $a-1$, and

$$\beta_n = \frac{(2n-1)\pi}{N_{\mathrm{C}}}, \quad n = 1, 2, \ldots, N_{\mathrm{C}} \tag{12}$$

are the abscissas of the Gauss–Chebyshev quadrature; see also [14, ch. 5.3]. For example, applying (10) and (11) to (6) yields

$$\begin{aligned} &p_y(y_k; \boldsymbol{\lambda}) \\ &\quad = \frac{1}{2\pi^2 \sigma^2 \Gamma(a) I_0(d)} \int_0^{2\pi} \exp[d\cos(\beta - c)]\, d\beta \\ &\qquad \cdot \int_0^{\infty} \exp\left[-\frac{|y_k - \sqrt{u/b} \cdot e^{j\beta}|^2}{\sigma^2}\right] u^{a-1} \exp(-u)\, du \\ &\quad \approx \frac{1}{\pi \sigma^2 \Gamma(a) N_{\mathrm{C}} I_0(d)} \sum_{n=1}^{N_{\mathrm{C}}} \exp[d\cos(\beta_n - c)] \\ &\qquad \cdot \sum_{i=1}^{N_{\mathrm{L}}} w_{\mathrm{L},i}(a-1) \exp\left[-\frac{|y_k - \sqrt{u_{\mathrm{L},i}(a-1)/b} \cdot e^{j\beta_n}|^2}{\sigma^2}\right]. \end{aligned} \tag{13}$$

To compute the derivatives in (9), we have also utilized the formulas in [11, (A.7) and (A.9)]. The (damped) Newton–Raphson algorithm updates the estimates of $\boldsymbol{\lambda}$ as follows (see, e.g., [14] and [15, (13.25)]:

$$\boldsymbol{\lambda}^{(i+1)} = \boldsymbol{\lambda}^{(i)} - \delta^{(i)} \cdot \left[\frac{\partial^2 L(\boldsymbol{\lambda}^{(i)}, \boldsymbol{y})}{\partial \boldsymbol{\lambda} \partial \boldsymbol{\lambda}^T}\right]^{-1} \frac{\partial L(\boldsymbol{\lambda}^{(i)}, \boldsymbol{y})}{\partial \boldsymbol{\lambda}} \tag{14}$$

where the damping factor $0 < \delta^{(i)} \leq 1$ is chosen (at every step i) to ensure that the log-likelihood function (7) increases, and the parameter estimates remain in the allowable parameter space $(a, b, d > 0)$. Initialization of the above iteration is discussed below.

A. Initialization

The above Newton–Raphson iteration can be initialized by neglecting the noise effects and using the following simple moment estimators of a and b:

$$a^{(0)} = \frac{(\hat{\mathrm{E}}[\alpha])^2}{\widehat{\mathrm{var}}(\alpha)} \tag{15a}$$

$$b^{(0)} = \frac{\hat{\mathrm{E}}[\alpha]}{\widehat{\mathrm{var}}(\alpha)} \tag{15b}$$

where

$$\hat{\mathrm{E}}[\alpha] = \frac{1}{K} \sum_{k=1}^{K} |y_k|^2, \quad \widehat{\mathrm{var}}(\alpha) = \frac{1}{K} \left[\sum_{k=1}^{K} |y_k|^4\right] - (\hat{\mathrm{E}}[\alpha])^2$$

and the following estimators of c and d (see [11, (2.2.4) and (5.3.11)]):

$$c^{(0)} = \begin{cases} \tan^{-1}(\bar{S}_y/\bar{C}_y), & \bar{C}_y \geq 0 \\ \tan^{-1}(\bar{S}_y/\bar{C}_y) + \pi, & \bar{C}_y < 0 \end{cases} \tag{15c}$$

$$d^{(0)} = \left(1.28 - 0.53 \cdot \bar{R}_y^2\right) \cdot \tan(\pi \bar{R}_y/2) \tag{15d}$$

where

$$\begin{aligned} \bar{R}_y &= \left(\bar{C}_y^2 + \bar{S}_y^2\right)^{1/2} \\ \bar{C}_y &= (1/K) \cdot \sum_{k=1}^{K} \cos(\angle y_k) \\ \bar{S}_y &= (1/K) \cdot \sum_{k=1}^{K} \sin(\angle y_k). \end{aligned}$$

B. Cramér–Rao Bounds

The CRB matrix for the unknown parameter vector $\boldsymbol{\lambda}$ can be computed by inverting the expected negative Hessian matrix, where the expectation is performed with respect to the distribution of $\mathbf{y}$ [16, ch. 3.7]:

$$\mathrm{CRB}_{\boldsymbol{\lambda}}(\boldsymbol{\lambda}) = -\left\{\mathrm{E}_{\boldsymbol{y}}\left[\frac{\partial^2 L(\boldsymbol{\lambda},\boldsymbol{y})}{\partial\boldsymbol{\lambda}\partial\boldsymbol{\lambda}^T}\right]\right\}^{-1}. \tag{16}$$

The above expectation requires multidimensional integration, which can be performed using Monte Carlo integration, i.e., by averaging $\partial^2 L(\boldsymbol{\lambda},\boldsymbol{y})/\partial\boldsymbol{\lambda}\partial\boldsymbol{\lambda}^T$ over many realizations of $\boldsymbol{y}$. The exact CRB in (16) does not have a closed-form expression, and it is, hence, difficult to predict its behavior as $\boldsymbol{\lambda}$ varies. Under the complete-data model, i.e., assuming that the signal amplitudes $\boldsymbol{\alpha}$ and phases β are *known*, we derive the *closed-form* complete-data CRB, which is a block-diagonal matrix:

$$\mathrm{CRB}_{\mathrm{c},\boldsymbol{\lambda}}(\boldsymbol{\lambda}) = \frac{1}{K}\cdot \mathrm{bdiag}\left\{\begin{bmatrix}\frac{\Gamma(a)\Gamma''(a)-[\Gamma'(a)]^2}{[\Gamma(a)]^2} & -1/b\\ -1/b & a/b^2\end{bmatrix}^{-1}, \frac{I_0(d)}{dI_1(d)}, \left[1-\left(\frac{I_1(d)}{I_0(d)}\right)^2-\frac{I_1(d)}{I_0(d)d}\right]^{-1}\right\}. \tag{17}$$

Clearly, the complete-data CRB is a lower bound on the exact CRB, i.e., $\mathrm{CRB}(\boldsymbol{\lambda}) - \mathrm{CRB}_{\mathrm{c}}(\boldsymbol{\lambda})$ is a positive semidefinite matrix.

Once the ML estimates of $\boldsymbol{\lambda}$ have been computed, we can utilize them to obtain MAP estimates of the amplitudes and phases of the eddy-current signal, as shown in the following section.

IV. MAP Estimation of Signal Amplitudes and Phases

Assume that the model parameters $\boldsymbol{\lambda}$ are *known*. We compute the MAP estimates of the signal amplitudes $\boldsymbol{\alpha} = [\alpha_1, \alpha_2, \ldots, \alpha_K]^T$ and phases $\boldsymbol{\beta} = [\beta_1, \beta_2, \ldots, \beta_K]^T$ by maximizing

$$\begin{aligned} L_{\mathrm{MAP}}(\boldsymbol{\alpha},\boldsymbol{\beta};\mathbf{y},\boldsymbol{\lambda}) &= \sum_{k=1}^{K}\ln[p_{y|\boldsymbol{\theta}}(y_k|\boldsymbol{\theta}_k)\cdot p_\alpha(\alpha_k;a,b)\cdot p_\beta(\beta_k;c,d)] \\ &= -K\ln(2\pi^2\sigma^2) - \left(\sum_{k=1}^{K}\frac{|y_k-\sqrt{\alpha_k}\cdot e^{j\beta_k}|^2}{\sigma^2}\right) \\ &\quad + Ka\ln b - K\ln\Gamma(a) \\ &\quad + (a-1)\cdot\left(\sum_{k=1}^{K}\ln\alpha_k\right) - b\left(\sum_{k=1}^{K}\alpha_k\right) \\ &\quad - K\ln I_0(d) + d\cdot\left[\sum_{k=1}^{K}\cos(\beta_k-c)\right]. \end{aligned} \tag{18}$$

For fixed $\boldsymbol{\beta}$, we can easily find the signal powers α that maximize (18):

$$\hat{\alpha}_k = \arg\max_{\alpha_k}\left[\sqrt{\alpha_k}\cdot y_k e^{-j\beta_k} + \sqrt{\alpha_k}\cdot y_k^* e^{j\beta_k} - (1+b\sigma^2)\cdot\alpha_k + (a-1)\sigma^2\cdot\ln\alpha_k\right]$$

where $k = 1, 2, \ldots, K$, and "*" denotes complex conjugation. Differentiating (18) with respect to α_k and solving for α_k yields (19a), shown at the bottom of the page. Similarly, for fixed $\boldsymbol{\alpha}$, the signal phases $\boldsymbol{\beta}$ that maximize (18) can be obtained as follows:

$$\hat{\beta}_k = \angle\left\{\sqrt{\alpha_k}\cdot y_k + \frac{1}{2}\cdot d\sigma^2\exp(jc)\right\}, \quad k = 1,2,\ldots,K. \tag{19b}$$

To obtain the MAP estimates of *both* $\boldsymbol{\alpha}$ and $\boldsymbol{\beta}$, iterate between (19a) and (19b) until convergence.

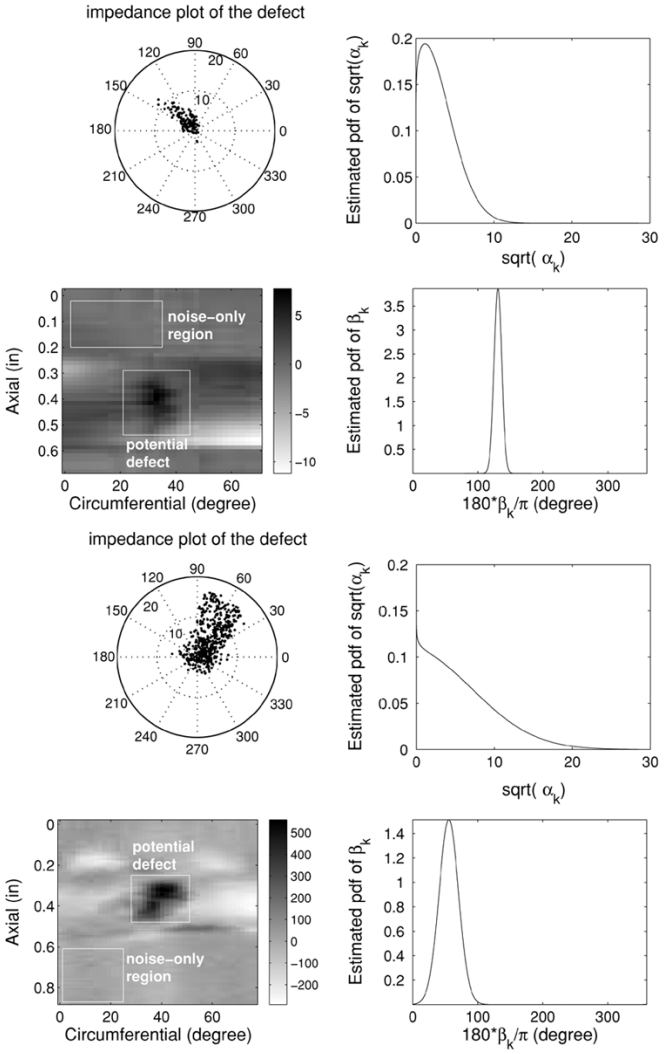

Fig. 4. (a) Impedance-plane and imaginary-component plots and (b) estimated amplitude and phase distributions of two potential defects.

V. Experimental and Simulation Results

We first apply the proposed ML estimation method to steam-generator inspection data containing two real defects. The tubes were made of Inconel 600 with outer diameter 0.875 in and wall thickness 0.050 in. We selected K measurements y_k, $k = 1, 2, \ldots, K$ from

$$\hat{\alpha}_k = \begin{cases}\left[\dfrac{\mathrm{Re}\{y_k\exp(-j\beta_k)\} + \{[\mathrm{Re}\{y_k\exp(-j\beta_k)\}]^2 + 4(a-1)\cdot\sigma^2(1+b\sigma^2)\}^{1/2}}{2(1+b\sigma^2)}\right]^2, & [\mathrm{Re}\{y_k\exp(-j\beta_k)\}]^2 \\ & \quad +4(a-1)\cdot\sigma^2(1+b\sigma^2) > 0 \\ 0, & [\mathrm{Re}\{y_k\exp(-j\beta_k)\}]^2 \\ & \quad +4(a-1)\cdot\sigma^2(1+b\sigma^2) < 0\end{cases} \tag{19a}$$

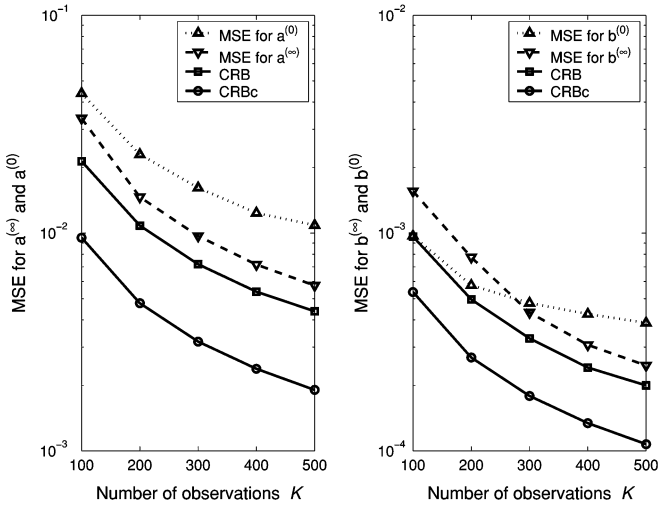

Fig. 5. MSEs and corresponding CRBs for amplitude distribution parameters a and b.

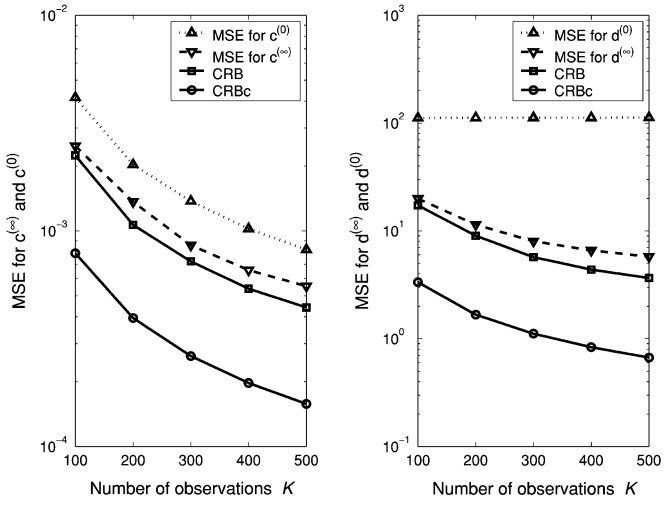

Fig. 6. MSEs and corresponding CRBs for phase distribution parameters c and d.

potential defect regions and estimated the noise variance σ^2 from neighboring regions that contain only noise. The quadrature orders of the Gauss–Chebyshev and generalized Gauss–Laguerre approximation were $N_{\mathrm{C}} = 120$ and $N_{\mathrm{L}} = 80$, respectively. The proposed algorithms converged within ten iterations. In Fig. 4, we show the estimated pdfs of the signal amplitudes $\sqrt{\alpha_k}$ and phases β_k. Here, the amplitudes $\rho_k = \sqrt{\alpha_k}$ follow the Nakagami-m pdf (see [12, (2.20)]:

$$p_\rho(\rho_k; a, b) = \frac{2b^a}{\Gamma(a)} \cdot \rho_k^{2a-1} \exp\left(-b\rho_k^2\right), \quad \rho_k \geq 0. \tag{20}$$

For the first test signal, the noise variance was $\sigma^2 = 1.9$, and the potential defect region contained $K = 154$ measurements. The ML estimate $\boldsymbol{\lambda}^{(\infty)}$ of the unknown parameter vector and the estimated covariance matrix of $\boldsymbol{\lambda}^{(\infty)}$ are shown in (21) at the bottom of the next page. For the second signal, $\sigma^2 = 1.9$ and $K = 525$, and $\boldsymbol{\lambda}^{(\infty)}$ and the estimated covariance matrix of $\boldsymbol{\lambda}^{(\infty)}$ are given in (22), shown at the bottom of the page. We have used (16) to compute the CRB matrix; the expectation with respect to the distribution of $\boldsymbol{y}$ was performed using Monte Carlo integration with 100 trials.

We now present a simulation example showing the estimation performance of the proposed method. Our performance metric is the mean-square error (MSE), calculated using 400 independent trials. The simulated data was generated using the measurement model in Section II with $\boldsymbol{\lambda} = [0.8, 0.14, 1.93, 13.2]$ and $\sigma^2 = 1.2$. In Figs. 5 and 6, we show the MSEs of

- the ML estimates of a, b and c, d, respectively, computed using the Newton–Raphson iteration (14) in Section III;
- the initial estimates (15a) and (15c) in Section III-A;

as well as corresponding exact and complete-data CRBs. The ML estimates performed well, achieving MSEs close to the exact CRBs. The initial estimates $a^{(0)}, b^{(0)}$, and $c^{(0)}$ performed fairly well, whereas $d^{(0)}$ performed poorly. The poor performance of $d^{(0)}$ can be explained by the fact that, being obtained by ignoring the noise effects, it cannot separate the phase variability of $y_k, k = 1, 2, \ldots, K$ due to the signal from that due to noise.

A. Empirical MAP Estimation of Signal Amplitudes and Phases

We apply the MAP estimator of signal amplitudes and phases (described in Section IV) to experimental eddy-current data, whose impedance-plane and magnitude plots are shown in Fig. 7(a) and (c). This data set was collected from the Electric Power Research

$$\boldsymbol{\lambda}^{(\infty)} = \begin{bmatrix} 0.548 \\ 0.0366 \\ 2.281 \\ 94.34 \end{bmatrix}$$

$$\mathrm{CRB}(\boldsymbol{\lambda}^{(\infty)}) = \begin{bmatrix} 6.29 \cdot 10^{-3} & 4.00 \cdot 10^{-4} & -8.01 \cdot 10^{-6} & -9.78 \cdot 10^{-2} \\ 4.00 \cdot 10^{-4} & 4.32 \cdot 10^{-5} & -1.42 \cdot 10^{-6} & 8.02 \cdot 10^{-3} \\ -8.02 \cdot 10^{-6} & -1.42 \cdot 10^{-6} & 6.22 \cdot 10^{-4} & -4.60 \cdot 10^{-2} \\ -9.78 \cdot 10^{-2} & 8.02 \cdot 10^{-3} & -4.60 \cdot 10^{-2} & 4.31 \cdot 10^{3} \end{bmatrix}. \tag{21}$$

$$\boldsymbol{\lambda}^{(\infty)} = \begin{bmatrix} 0.4765 \\ 0.0083 \\ 0.9676 \\ 14.65 \end{bmatrix}$$

$$\mathrm{CRB}(\boldsymbol{\lambda}^{(\infty)}) = \begin{bmatrix} 3.85 \cdot 10^{-3} & 6.48 \cdot 10^{-5} & -2.50 \cdot 10^{-5} & -5.93 \cdot 10^{-3} \\ 6.48 \cdot 10^{-5} & 2.09 \cdot 10^{-6} & -1.07 \cdot 10^{-7} & 2.94 \cdot 10^{-5} \\ -2.50 \cdot 10^{-5} & -1.07 \cdot 10^{-7} & 8.99 \cdot 10^{-4} & -4.07 \cdot 10^{-3} \\ -5.93 \cdot 10^{-3} & 2.94 \cdot 10^{-5} & -4.07 \cdot 10^{-3} & 7.9538 \end{bmatrix}. \tag{22}$$

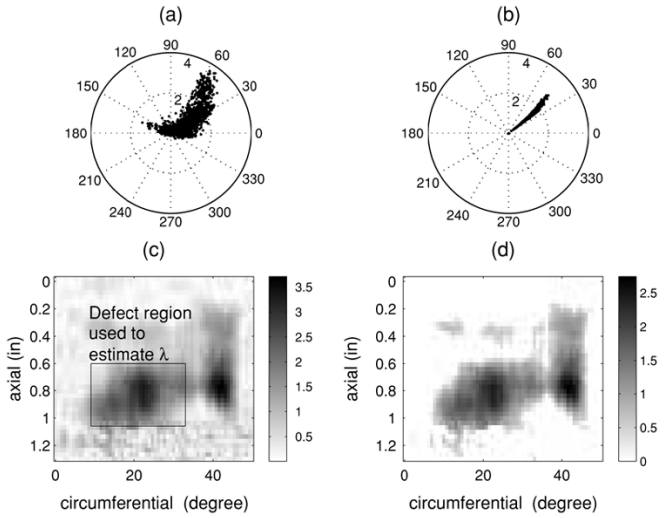

Fig. 7. Impedance-plane and magnitude plots of (a) original eddy-current data and (b) corresponding empirical MAP estimates.

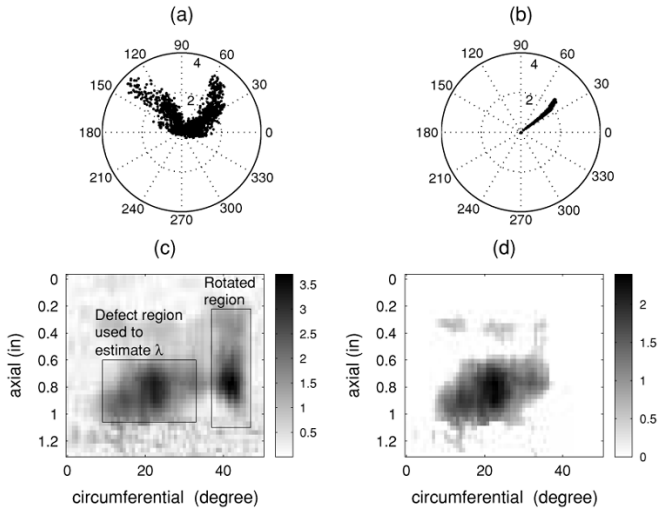

Fig. 8. Impedance-plane and magnitude plots of eddy-current data with the axial defect signal's phases rotated by (a) -70° and (b) corresponding empirical MAP estimates.

Institute's laboratory sample 3 made of Inconel 600. The sample contained two machined defects: a 49% throughwall circumferential OD defect and a 59% throughwall axial OD defect. We first estimate the model parameters $\boldsymbol{\lambda}$ from a *training region* containing defects of the type that we wish to detect and then apply the proposed MAP method to the whole image. In this example, we selected the training region containing the 49% circumferential OD defect. In the MAP algorithm, we replaced $\boldsymbol{\lambda}$ with its ML estimate obtained from the training region (in the spirit of empirical Bayesian estimation). The impedance-plane and magnitude plots of the resulting *empirical MAP estimates* are shown in of Fig. 7(b) and (d). The empirical MAP estimator *enhances* potential defect signals having similar amplitude and phase distributions to those estimated from the training region and *suppresses* other signals. To show this effect, we have rotated the phases of the 59% throughwall axial defect signals by -70°, yielding the impedance-plane and magnitude plots in Fig. 8(a) and (c). Clearly, Figs. 7(c) and 8(c) are identical because phase rotation does not affect the signal magnitudes. After applying the proposed empirical MAP estimator, the rotated defect signals are completely suppressed, as shown in Fig. 8(b) and (d).

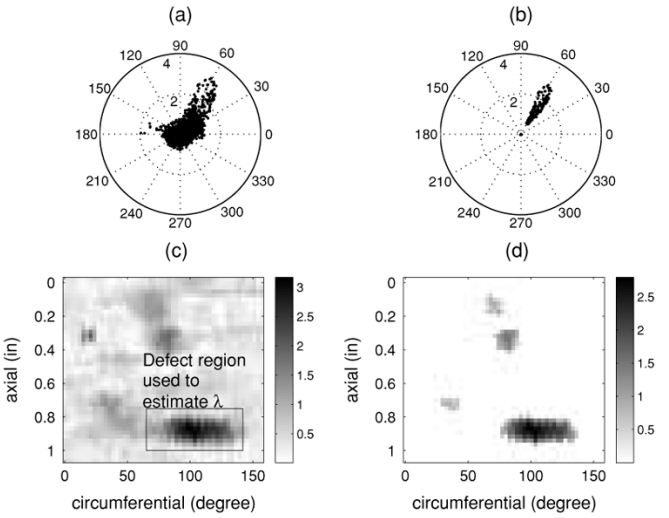

Fig. 9. Impedance-plane and magnitude plots of (a) original eddy-current data and (b) corresponding empirical MAP estimates.

Finally, we apply the empirical MAP estimator to a data set containing real defect signals and show the obtained results in Fig. 9

VI. Concluding Remarks

We developed a statistical model for characterizing the amplitude and phase probability distributions of potential defects in eddy-current systems and derived a maximum likelihood method for estimating the unknown parameters from noisy measurements. We also discussed initializing the proposed algorithm and computed exact and complete-data Cramér–Rao bounds for the unknown parameters. We showed how the estimated amplitude and phase distribution parameters can be utilized for maximum *a posteriori* signal phase and amplitude estimation. The proposed methods were applied to simulated and real data from steam-generator tube inspection in nuclear power plants.

Further research will concentrate on utilizing the estimated amplitude and phase distribution parameters as feature extractors in defect classification schemes.

References

[1] B. A. Auld and J. C. Moulder, "Review of advances in quantitative eddy current nondestructive evaluation," *J. Nondestructive Eval.*, vol. 18, no. 1, pp. 3–36, Mar. 1999.

[2] P. Cawley, "Non-destructive testing—Current capabilities and future directions," in *Proc. Inst. Mech. Engrs.*, vol. 215, Nov. 2001, pp. 213–223.

[3] L. Udpa and W. Lord, "New approaches for multifrequency eddy current testing of steam generator tubes," in *Proc. ISMM Int. Symp.*. Honolulu, HI, Feb. 1988, pp. 108–112.

[4] P. Xiang, S. Ramakrishnan, X. Cai, P. Ramuhalli, R. Polikar, S. S. Udpa, and L. Udpa, "Automated analysis of rotating probe multi-frequency eddy current data from steam generator tubes," *Int. J. Applied Electromag. Mech.*, vol. 12, pp. 151–164, 2000.

[5] C. V. Dodd and W. E. Deeds, "Analytical solutions to eddy current probe-coil problems," *J. Appl. Phys.*, vol. 39, pp. 2829–2838, May 1968.

[6] E. E. Kriezis, T. D. Tsiboukis, S. M. Panas, and J. A. Tegopoulos, "Eddy currents: Theory and applications," *Proc. IEEE*, vol. 80, no. 10, pp. 1559–1589, Oct. 1992.

[7] C. S. Antonopoulos and T. D. Tsiboukis, "Field calculation in single- and multilayer coaxial cylindrical shells of infinite length by using a coupled $\bar{T} - \Omega$ and boundary element method," *IEEE Trans. Magn.*, vol. 28, no. 1, pp. 61–66, Jan. 1992.

[8] G. Micolau, G. Pichenot, D. Premel, D. Lesselier, and M. Lambert, "Dyad-based model of the electric field in a conductive cylinder at eddy-current frequencies," *IEEE Trans. Magn.*, vol. 40, no. 3, pp. 400–409, Mar. 2004.

[9] A. Dogandvžić and P. Xiang, "A statistical model for eddy-current defect signals from steam generator tubes," in *Proc. 30th Annu. Review Progress Quantitative Nondestructive Evaluation*, Green Bay, WI, July 2003, pp. 605–612.
[10] A. Viterbi, "Optimum detection and signal selection for partially coherent binary communication," *IEEE Trans. Inf. Theory*, vol. IT-11, no. 2, pp. 239–246, Apr. 1965.
[11] K. V. Mardia and P. E. Jupp, *Directional Statistics*. New York: Wiley, 2000.
[12] M. K. Simon and M.-S. Alouini, *Digital Communication Over Fading Channels*. New York: Wiley, 2000.
[13] M. K. Simon, S. M. Hinedi, and W. C. Lindsey, *Digital Communication Techniques-Signal Design and Detection*. Englewood Cliffs, NJ: Prentice-Hall, 1995.
[14] R. A. Thisted, *Elements of Statistical Computing: Numerical Computation*. New York: Chapman & Hall, 1988.
[15] G. A. F. Seber and C. J. Wild, *Nonlinear Regression*. New York: Wiley, 1989.
[16] S. M. Kay, *Fundamentals of Statistical Signal Processing—Estimation Theory*. Englewood Cliffs, NJ: Prentice-Hall, 1993.

Correction to "Universal Trellis Codes for Diagonally Layered Space-Time Systems"

Adina Matache, *Student Member, IEEE* and
Richard D. Wesel, *Senior Member, IEEE*

Fig. 1 replaces the incorrect [1, Fig. 3]. The simulation results are unchanged, but the computation of α was incorrect, leading to some improperly plotted points in [1, Fig. 3]. Although the corrected graph is somewhat different, it does not affect the discussion or conclusion.

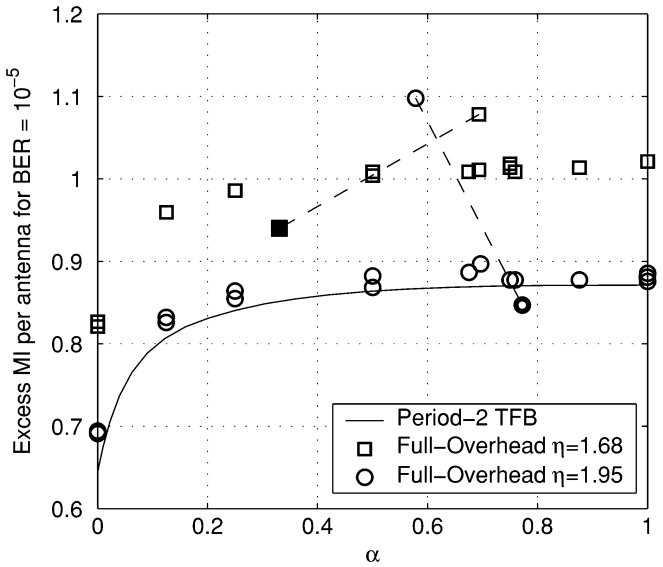

Fig. 1. Excess MI per antenna required by rate-1/3, 8-PSK trellis code #1 to achieve BER $= 10^{-5}$ versus the ratio of periodic SNRs $\alpha = \gamma_2^{\mathrm{MMSE}}/\gamma_1^{\mathrm{MMSE}}$.

Manuscript received July 29, 2004; revised October 26, 2004. The associate editor coordinating the review of this manuscript and approving it for publication was Dr. Helmut Boelcskei.

The authors are with the Department of Electrical Engineering, University of California, Los Angeles, CA 90095 USA.

Digital Object Identifier 10.1109/TSP.2005.851182

References

[1] A. Matache and R. D. Wesel, "Universal trellis codes for diagonally layered space-time systems," *IEEE Trans. Signal Process. Special Issue on MIMO Wireless Communications*, vol. 51, no. 11, pp. 2773–2783, Nov. 2003.

Comments on "Estimation of Frequencies and Damping Factors by Two-Dimensional ESPRIT Type Methods"

Yang Wang, Jian-Wen Chen, and Zhong Liu

***Index Terms*—ESPRIT-type algorithm, pairing procedures, permutation matrices, two-dimensional signals.**

In [1], the authors present two high-resolution approaches to estimate two-dimensional (2-D) signal parameters. The first approach (see also [2]) decomposes the 2-D estimation problem into two one-dimensional (1-D) ones, estimates the 1-D frequencies with the MEMP method [3], and then forms correct pairs using a new pairing scheme introduced in [4]. The second method (the 2-D ESPRIT method) directly estimates the 2-D frequencies. It is shown that both methods are more accurate than the related methods. The paper has been read with great interest; however, it appears to have a key error in the permutation matrix specification of the first method. In this comment, we derive the correct one with the performance simulations.

For convenience, let [1, ( )] denote the equations in the original paper. The permutation matrices defined by [1, (47)] read as

$$\begin{cases} P_1 = T^{-1}T_a \\ P_2 = T^{-1}T_b. \end{cases} \tag{47}$$

It is pointed out here that this definition is not accurate. The correct one should be[1]

$$\begin{cases} P_1 = TT_a^{-1} \\ P_2 = TT_b^{-1} \end{cases}. \tag{1}$$

Equation (1) can be reasoned as follows. Using [1, (40) and (42)] yields

$$\begin{cases} \Phi_1 = TF_1T^{-1} \\ \Phi_2 = TF_2'T^{-1}. \end{cases} \tag{2}$$

The main diagonals of Φ_1 and Φ_2 are ordered frequencies and damping factors. Therefore, the eigenvalue decompositions of F_1 and F_2' in [1, (45)] should be denoted by

$$\begin{cases} F_1 = T_a^{-1}\Phi_a T_a \\ F_2' = T_b^{-1}\Phi_b T_b \end{cases} \tag{3}$$

Manuscript received June 6, 2004; revised September 22, 2004. The associate editor coordinating the review of this manuscript and approving it for publication was Prof. Mats Viberg.

Y. Wang and Z. Liu are with the Department of Electronic Engineering, Nanjing University of Science and Technology, Nanjing, Jiangsu 210094, China (e-mail: wangyang412@sohu.com; zhongliu@mail.njust.edu.cn).

J.-W. Chen is with the Nanjing Research Institute of Electronics Technology, Nanjing, Jiangsu 210013, China (e-mail: cjwll8217@sina.com).

Digital Object Identifier 10.1109/TSP.2005.851184

[1] At first, we thought this was a typing error; however, [2] uses the same permutation matrices.